Eur. Phys. J. C 48, 531–543 (2006)
DOI 10.1140/epjc/s10052-006-0052-2

THE EUROPEAN PHYSICAL JOURNAL C

Regular Article – Theoretical Physics

Lattice QCD constraints on the nuclear equation of state

A.S. Khvorostukhin[1,2,a], V.V. Skokov[1,2,b], V.D. Toneev[1,2,c], K. Redlich[1,3,d]

[1] Gesellschaft für Schwerionenforschung mbH, Planckstr. 1, 64291 Darmstadt, Germany
[2] Joint Institute for Nuclear Research, 141980 Dubna, Moscow Region, Russia
[3] University of Wroclaw, 50204 Wroclaw, Poland

Received: 26 June 2006 / Revised version: 7 September 2006 /
Published online: 24 October 2006 –

Abstract. Based on the quasi-particle description of the QCD medium at finite temperature and density we formulate the phenomenological model for the equation of state that exhibits crossover or the first-order deconfinement phase transition. The models are constructed in such a way as to be thermodynamically consistent and to satisfy the properties of the ground state nuclear matter complying with constraints from intermediate heavy-ion collision data. Our equations of states show a quite reasonable agreement with the recent lattice findings on the temperature and baryon chemical potential dependence of relevant thermodynamical quantities in the parameter range covering both the hadronic and quark–gluon sectors. The model predictions on the isentropic trajectories in the phase diagram are shown to be consistent with the recent lattice results. Our nuclear equations of state are to be considered as an input to the dynamical models describing the production and the time evolution of a thermalized medium created in heavy-ion collisions in a broad energy range from SIS up to LHC.

PACS. 21.65.+f; 24.85.+p; 12.38.Aw; 12.38.Mh

1 Introduction

QCD at the finite temperature T and/or baryon chemical potential $\mu_{\rm B}$ is of fundamental importance, since it describes the relevant features of particle physics in the early universe, in neutron stars and in heavy-ion collisions (see e.g. [1, 2]). With the relativistic heavy-ion collision experiments at the AGS, SPS and RHIC accelerators one explores the phase diagram of strongly interacting matter in a broad parameter range of temperature and baryon density. Lattice QCD results on the equation of state (EoS) of QCD matter provide a basic input for the analysis of experimental signatures of the possible quark–gluon plasma formation in heavy-ion collisions. Directly addressing the EoS, the hydrodynamics realizes the connection between the matter properties and observables. The hydrodynamic treatment of the whole time evolution of colliding nuclei requires knowledge of the nuclear EoS within a large interval of its thermodynamic variables covering both the quark–gluon and hadronic sectors.

In recent years significant progress has been made in understanding the phase diagram of QCD at non-zero baryon chemical potential as the non-perturbative lattice QCD methods were extended to access the relevant regions of the phase diagram. Recently, the first lattice calculations have been performed for a non-vanishing T and $\mu_{\rm B}$ for systems with $N_f = 2$ [3, 4] and $N_f = 2+1$ [5, 6] flavors. However, due to a set of approximations the lattice gauge theory (LGT) is still not able to provide results on the properties of the hadronic matter in the confined phase. LGT is also restricted to moderate values of the baryon chemical potential $\mu_{\rm B}$ such that $\mu_{\rm B} \lesssim T$. That is why different phenomenological models are required to describe the thermodynamic properties and equation of state of QCD matter for larger baryon densities. Obviously, such models depend on the set of parameters that are usually fixed to reproduce the existing LGT results as well as the basic phenomenological properties of the nuclear matter obtained from the experimental data. Recently, the thermodynamics of the quark–gluon phase was interpreted quite successfully within the QCD inspired massive quasi-particle models [7–17]. On the other hand, as demonstrated by lattice calculations, a rapid growth of the energy density ε and pressure p when approaching the critical temperature $T_{\rm c}$ was shown to be reproduced in terms of the hadron resonance gas model with scaled masses [20–22]. Only recently there have been attempts to describe lattice QCD thermodynamics both above and below $T_{\rm c}$ in terms of a field theoretical model, including the fea-

[a] e-mail: hvorost@theor.jinr.ru
[b] e-mail: vvskokov@theor.jinr.ru
[c] e-mail: V.Toneev@gsi.de
[d] e-mail: redlich@ift.uni.wroc.pl

tures of both deconfinement and chiral symmetry restoration [23], as well as within some phenomenological models that are based on lattice QCD results for the quark–gluon partition function [24]. Some unique parametrization of the QCD EoS below and above T_c was also presented in [25].

The phenomenological equation of state should not only be thermodynamically consistent [26] but should also be capable to reproduce the global behavior of the nuclear matter near the ground state and its saturation properties. In addition, there are experimental restrictions coming from the flow analysis in heavy-ion collisions which limit the acceptable theoretical values of pressure in a finite interval of baryon densities n_B at $T = 0$ [27, 28]. Some constraints on the EoS are also imposed through the analysis of cold charge-neutral baryonic matter in β-equilibrium compact stars [29, 30]. There are also essential constraints on the model properties coming from the recent LGT results.

In this paper, we will construct the EoS of strongly interacting QCD matter with a deconfinement phase transition that satisfies the above mentioned hadronic constraints and those imposed by the recent lattice QCD results obtained for the $(2+1)$-flavor system at finite T and non-vanishing baryonic chemical potential.

This paper is organized as follows: In Sect. 2 we introduce the quasi-particle model for the EoS with a deconfinement phase transition. In Sect. 3 the model predictions are compared with the recent lattice data obtained in $(2+1)$-flavor QCD at the finite T and μ_B. Our results and comments on the properties of the QCD equation of state and thermodynamics are summarized in the last section.

2 The equation of state

Lattice results show that even at temperature T much larger than deconfinement temperature T_c the thermodynamical observables like pressure or entropy, baryon number and energy density are still by $\gtrsim 20\%$ deviating from their asymptotic ideal-gas values. Such deviations, observed at $T > 2T_c$, were shown to be well understood by a systematic contribution in the self-consistent implementation of quasi-particle masses in the HTL-resummed perturbative QCD [31]. On the other hand, the LGT thermodynamics below T_c was shown to be well reproduced by the hadron resonance gas partition function [20–22]. To possibly describe the thermodynamics at $T = T_c$ or near the phase transition additional model assumptions are required [11, 32–34].

It is clear from the above that a straightforward model for the QCD EoS can be constructed by connecting a non-interacting hadron resonance gas in the low temperature phase with an ideal quark–gluon plasma in some non-perturbative bag for the color deconfined phase [13]. These phases are matched at the phase transition boundary by means of the Gibbs phase equilibrium condition. By construction, this approach yields the first-order phase transition. Such a MIT-bag-like model [35] is so far the simplest method to implement the confinement phenomenon in the EoS, though it has some serious shortcomings.

A more complete method to model the QCD EoS is based on the effective Hamiltonian that includes interactions of the constituents. In the quasi-particle approximation such a Hamiltonian can be modeled through density-dependent mean-field interactions [26, 36–38]:

$$H = \sum_{j\in h,q,g} \sum_{s} \int \mathrm{d}\mathbf{r} \psi_j^+(\mathbf{r},s) \left(\sqrt{-\nabla^2 + m_i^2} + U_j(\rho) \right) \times \psi_j(\mathbf{r},s) - C(\rho)\cdot V\,, \tag{1}$$

where j enumerates different species of quasi-particles (hadrons and/or unbound quarks and gluons) and s stands for their internal degrees of freedom. Here $U_j(\rho)$ is the density-dependent mean-field acting on the quasi-particle j described by the field operator ψ_j with m_j being the current mass of quarks and gluons or the free mass of hadrons. Applying the density-dependent Hamiltonian (1) in the partition function requires some additional constraints that are needed to fulfill the thermodynamic consistency condition [39–41]:

$$\left\langle \frac{\partial H}{\partial T} \right\rangle = 0\,, \quad \left\langle \frac{\partial H}{\partial \rho_j} \right\rangle = 0\,, \tag{2}$$

where $\langle A \rangle$ denotes the average value of the operator A over the statistical ensemble. With the Hamiltonian (1) the conditions (2) can be also expressed as [39–41]

$$\sum_j \rho_j \frac{\partial U_j}{\partial \rho_i} - \frac{\partial C}{\partial \rho_i} = 0\,, \sum_j \rho_j \frac{\partial U_j}{\partial T} - \frac{\partial C}{\partial T} = 0\,. \tag{3}$$

It can be shown [26, 36–38] that the conditions (3) are satisfied only if the mean field $U_j(\rho)$ and the correcting function $C(\rho)$ are temperature independent.

In the following, we consider the basic structure of the effective Hamiltonian (1) to model the EoS of hadronic and quark–gluon plasma phase.

2.1 The hadronic phase

The hadronic phase is considered as a gas of hadrons and resonances in the thermodynamic equilibrium. In general, the particle density of species j is obtained from

$$n_j \equiv n_j(T, \mu_j - U_j) = \frac{d_j}{2\pi^2} \int_0^\infty \mathrm{d}k k^2 f_j(k, T, \mu_j - U_j)\,, \tag{4}$$

where the one-particle distribution function with an argument z is

$$f_j(k,T,z) = \left[\exp\left(\frac{\sqrt{k^2+m_j^2} - z}{T} \right) + \mathcal{L}_j \right]^{-1}\,, \tag{5}$$

with $\mathcal{L}_j = +1$ for fermions and $\mathcal{L}_j = -1$ for bosons, while d_j is the spin–isospin degeneracy factor. The chemical potential μ_j is related to the baryon (μ_B) and the strangeness (μ_S) chemical potentials by

$$\mu_j = b_j \mu_\mathrm{B} + s_j \mu_\mathrm{S} \,, \tag{6}$$

with b_j and s_j being the baryon number and strangeness of the particle j. The hadronic potential $U_j \equiv U_j^{(h)}$ is described by a non-linear mean-field model [42]:

$$U_j^{(h)} = g_{r,j}\varphi_1(x) + g_{a,j}\varphi_2(y) \,, \tag{7}$$

where $g_{r,j} > 0$ and $g_{a,j} < 0$ are repulsive and attractive coupling constants, respectively. The effect of interactions results also in an additional density-dependent term $C(\rho)$ that contributes to the thermodynamic pressure and energy densities. If the particle interaction is taken in form of (1), the thermodynamic consistency implies that the functions $\varphi_1(x)$ and $\varphi_2(y)$ depend only on particle densities. In [42] these functions were chosen such that

$$b_1\varphi_1 = x \,, \quad -b_1\left(\varphi_2 + b_2\varphi_2^3\right) = y \,, \tag{8}$$

where

$$x = \sum_i g_{r,i} n_i \,, \quad y = \sum_i g_{a,i} n_i \,,$$

with b_1 and b_2 being free parameters. The φ_2^3 term is introduced to get a slower than linear increase of attraction with density at a high compression as it happens in the relativistic mean-field models. Having in mind that the hadronic EoS will be compared with that of the quark–gluon plasma, it is convenient to rewrite (8) in terms of a number of constituent quarks and antiquarks ν_i:

$$\rho_j = \nu_j n_j \equiv \nu_j n_j(T, \mu_j - U_j) \,. \tag{9}$$

In the original paper [42], the hadronic phase was modeled as a mixture of nucleons and Δ's (i.e. $j = N, \Delta$). Following [26], we generalize this approach by including all hadrons and resonances with a mass up to 1.6 GeV. One also assumes that all coupling constants scale with the number of constituent quarks [26]:

$$U_j^{(h)} = \nu_j \left(\left[\widetilde{\varphi}_1(\rho^{(h)}) \right]^\alpha + \widetilde{\varphi}_2(\rho^{(h)}) \right) , \tag{10}$$

where $\widetilde{\varphi}_1$ and $\widetilde{\varphi}_2$ satisfy (8) in the following form:

$$c_1\widetilde{\varphi}_1^\alpha = \rho^{(h)} \,, \quad -c_2\widetilde{\varphi}_2 - c_3\widetilde{\varphi}_2^3 = \rho^{(h)} \,, \tag{11}$$

with $\rho^{(h)} = \sum_j \nu_j \rho_j = 3\sum_\mathrm{B} n_j + 2\sum_M n_j$. As compared to (8) a free parameter α is also introduced in (10). This parameter is used to control the strength of the repulsive interactions at high density [36–38]. The parameters in (11) are expressed as [36, 37]

$$c_1 = \frac{b_1}{(g_{r,j}/\nu_j)^2} \,, \quad c_2 = \frac{b_1}{(g_{a,j}/\nu_j)^2} \,, \quad c_3 = \frac{b_1 b_2}{(g_{a,j}/\nu_j)^4} \,,$$

and they are fixed by requiring that the properties of the ground state ($T = 0$ and $n_\mathrm{B} = n_0 \approx 0.15\,\mathrm{fm}^{-3}$) of the nuclear matter are reproduced: zero pressure, binding energy per nucleon of -16 MeV and incompressibility of 210 MeV.

Solving the cubic equation (11), one gets the interaction potential thus:

$$U_j^{(h)} = \nu_j \left[\frac{1}{c_1}(\rho^{(h)})^\alpha - F(\rho^{(h)}) \right] , \tag{12}$$

where the function F depends on the density of quarks bounded inside hadrons as follows:

$$F(t) = \frac{12^{1/3}}{6}\eta - 2\beta\eta^{-1} \quad \text{with} \quad \eta = \left(\frac{t}{a} + \sqrt{\beta^3 + \frac{t^2}{a^2}} \right)^{\frac{1}{3}} . \tag{13}$$

Here a, β are proportional to the coefficients of the (11): $a = c_3/9$ and $\beta = c_2/12^{1/3}$.

In this representation we obtained for the hadronic pressure

$$p^{(\mathrm{H})}\left(T, \mu_j - U_j^{(h)}\right) = \sum_{j\in h} \frac{d_j}{6\pi^2} \int_0^\infty \frac{k^2}{\sqrt{k^2 + m_j^2}} \times f_j\left(k, T, \mu_j - U_j^{(h)}\right) k^2 \,\mathrm{d}k + C(\rho^{(h)}) \tag{14}$$

and for the energy density

$$\varepsilon^{(H)}\left(T, \mu_j - U_j^{(h)}\right) = \sum_{j\in h} \frac{d_j}{2\pi^2} \int_0^\infty \left(\sqrt{k^2 + m_j^2} + U_j^{(h)} \right) f_j \times \left(k, T, \mu_j - U_j^{(h)}\right) k^2 \,\mathrm{d}k - C(\rho^{(h)}) \,, \tag{15}$$

where the function C is obtained from

$$C(\rho^{(h)}) = \frac{1}{c_1}\frac{\alpha}{\alpha+1}(\rho^{(h)})^\alpha - \rho^{(h)} F(\rho^{(h)}) + \int_0^{\rho^{(h)}} F(t)\,\mathrm{d}t \,. \tag{16}$$

As shown in Fig. 1, the above hadronic EoS satisfies the constraint resulting from the nucleon flow analysis of heavy-ion collisions in the energy range $\lesssim 10$ AGeV. The upper boundary of the shaded area is consistent with the constraint coming from the analysis of the neutron star properties [30]. In the high-temperature regime there is also a reasonable agreement of our model with the thermodynamics of the interacting pion gas from [43] (see Fig. 2).

2.2 The two-phase bag model

In the MIT-bag-like model, the deconfinement phase transition is determined by matching the EoS of an ideal relativistic gas of hadrons and resonances to that of an ideal

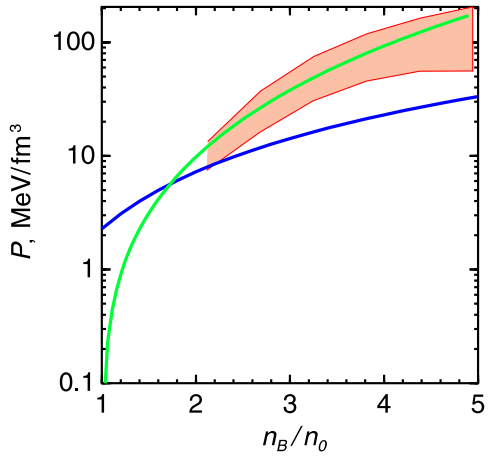

Fig. 1. Pressure as a function of baryon density for $T = 0$. *Grey* and *black solid lines* are calculated for the modified Zimanyi model and ideal gas EoS, respectively. The *shaded region* corresponds to the Danielewicz et al. constraint [27, 28]

gas of quarks and gluons. In the following we consider the two-phase (2P) model that accounts for interactions separately in the hadronic and quark–gluon plasma phase. The hadronic phase is described within the phenomenological mean-field model introduced in the previous section. Following (4), the total baryon density and the strangeness density in the hadronic phase can be expressed as

$$n_{\rm B}^{\rm H} = \sum_{j\in h} b_j\, n_j \left(T, \mu_j - U_j^{(h)}\right) , \tag{17}$$

$$n_{\rm S}^{\rm H} = \sum_{j\in h} s_j\, n_j \left(T, \mu_j - U_j^{(h)}\right) , \tag{18}$$

where the sum is taken over all hadrons and resonances. Similarly, the pressure and energy density of the species j are given by (14) and (15).

In the quasi-particle approximation, the QGP phase is commonly described as a gas of partons (non-interacting point-like quarks, antiquarks and gluons) confined in a "bag". The non-perturbative effects associated with confinement are presented by the constant vacuum energy B. The recent LGT results show that such an approach is not adequate as the EoS differs from the asymptotic ideal-gas values even at temperatures as high as $100T_{\rm c}$ [44]. The perturbative QCD results can, however, be improved through the so-called hard thermal loop (HTL) expansion. According to the HTL perturbative expansion, the QCD thermodynamics at high temperature is controlled by quasi-particles with a temperature dependent mass $m_q(T)$. For $\mu_{\rm B} = 0$ one gets [44–46]

$$m_q^2(T) - m_{q0}^2 = \frac{N_g}{16Nc} T^2 g^2 . \tag{19}$$

To model the HTL results within the mean-field approach one introduces the quark and gluon potentials to reproduce the behavior of the HTL masses (19) in the high-temperature limit. This in general results in an additional equation for the unknown gluon density. To simplify the problem we modify the potential so that it coincides only with the HTL expression for quarks. In the high-temperature limit and having in mind that $\rho \sim T^3$, the simplest phenomenological choice of the potential is

$$U^{(\rm pl)} = \mathcal{B}(\rho^{(\rm pl)})^{1/3} , \tag{20}$$

where $\mathcal{B}$ is obtained comparing the asymptotic expansion of (20) with the HTP result

$$\mathcal{B} = g \frac{\sqrt{\frac{N_g}{16N_c}}}{\left(\frac{\zeta(3)}{2\pi^2}\left(2d_g + 3N_f d_q\right)\right)^{1/3}} , \tag{21}$$

with d_q and d_g being the degeneracy factors for quarks and gluons, respectively. For $N_c = 3$ and $N_g = 8$ one gets

$$\mathcal{B}(N_f = 3) = 0.2351g , \tag{22}$$

$$\mathcal{B}(N_f = 2) = 0.2542g , \tag{23}$$

where the strong interaction coupling constant g is treated as a free parameter.

The thermodynamic self-consistency conditions require that the mean-field contribution to the pressure and energy

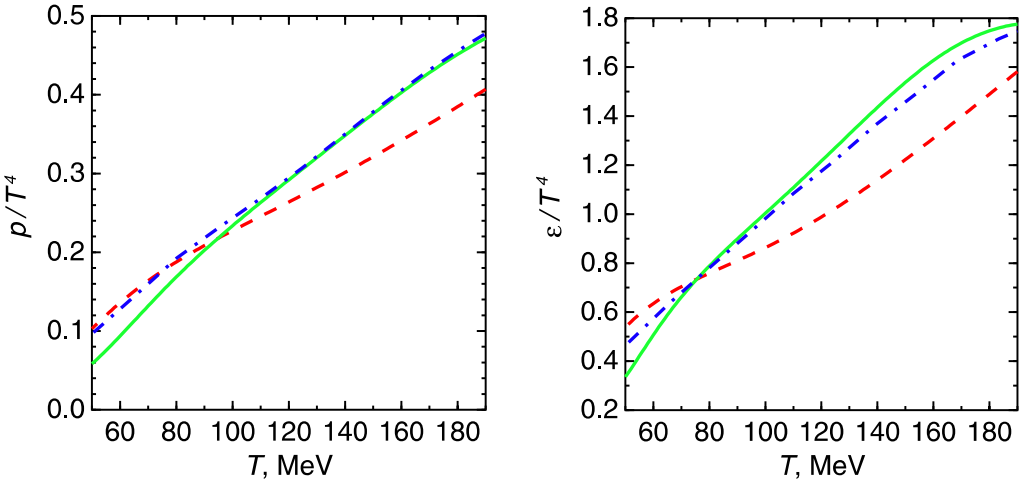

Fig. 2. Temperature dependence of the reduced pressure and energy density for an interacting pion gas ($\pi + \rho$ system). The *solid line* is our result, *dash-dotted* and *dashed ones* are the interacting [43] and ideal pion gas, respectively

density in equations like (14) and (15) is respectively

$$U_i^{(\mathrm{pl})} = \mathcal{B}\nu_i(\rho^{(\mathrm{pl})})^{1/3}\,, \tag{24}$$

$$C(\rho^{(\mathrm{pl})}) = \frac{\mathcal{B}}{4}(\rho^{(\mathrm{pl})})^{4/3} + B\,, \tag{25}$$

where the plasma particle density $\rho^{(\mathrm{pl})} = \sum_{j\in g,q,\bar{q}} \rho_j$ and the bag constant B is included in the correcting function C.

With such mean-field potentials the pressure and energy density in the plasma phase carried by u, d and s quarks and antiquarks is obtained:

$$p^Q\left(T, \mu_j - U_j^{(\mathrm{pl})}\right) = \sum_{j\in g,q,\bar{q}} p_j\left(T, \mu_j - U_j^{(\mathrm{pl})}\right) - C(\rho^{(\mathrm{pl})})\,, \tag{26}$$

$$\varepsilon^Q\left(T, \mu_j - U_j^{(\mathrm{pl})}\right) = \sum_{j\in g,q,\bar{q}} \varepsilon_j\left(T, \mu_j - U_j^{(\mathrm{pl})}\right) + C(\rho^{(\mathrm{pl})})\,. \tag{27}$$

To quantify these observables we use the quark masses $m_u = m_d = 65\,\mathrm{MeV}$ and $m_s = 135\,\mathrm{MeV}$, the gluon mass $m_g = 700\,\mathrm{MeV}$ and the bag constant $B^{1/4} = 207\,\mathrm{MeV}$. Such parameters yield a transition temperature $T_\mathrm{c} \approx 170\,\mathrm{MeV}$ in agreement with the recent lattice result obtained for the vanishing net baryon number [2]. For massless gluons the equation of state has the simple form

$$p_g(T) = \frac{d_g\pi^2}{90}T^4\,, \quad \varepsilon_g(T) = 3p_g(T) = \frac{d_g\pi^2}{30}T^4\,, \quad \text{with} \quad d_g = 16\,. \tag{28}$$

The baryon number and strangeness density in the quark–gluon plasma are obtained following (17) and (18) from

$$n_\mathrm{B}^\mathrm{Q} = \sum_{j\in g,q,\bar{q}} b_j n_j\left(T, \mu_j - U_j^{(\mathrm{pl})}\right)\,, \tag{29}$$

$$n_\mathrm{S}^\mathrm{Q} = \sum_{j\in g,q,\bar{q}} s_j n_j\left(T, \mu_j - U_j^{(\mathrm{pl})}\right)\,. \tag{30}$$

The equilibrium between the plasma and the hadronic phase is determined by the Gibbs conditions for the thermal ($T^\mathrm{Q} = T^\mathrm{H}$), mechanical ($p^\mathrm{Q} = p^\mathrm{H}$) and chemical ($\mu_\mathrm{B}^\mathrm{Q} = \mu_\mathrm{B}^\mathrm{H},\ \mu_\mathrm{S}^\mathrm{Q} = \mu_\mathrm{S}^\mathrm{H}$) equilibrium. At a given temperature T and baryon chemical potential μ_B the strange chemical potential μ_S is obtained by requiring that the net strangeness of the total system vanishes. Consequently, the phase equilibrium condition and strangeness conservation imply that

$$p^\mathrm{H}\left(T, \mu_j - U_j^{(h)}\right) = p^\mathrm{Q}\left(T, \mu_j - U_j^{(\mathrm{pl})}\right)\,, \tag{31}$$

$$n_\mathrm{B} = \lambda n_\mathrm{B}^\mathrm{Q}\left(T, \mu_j - U_j^{(\mathrm{pl})}\right) + (1-\lambda)n_\mathrm{B}^\mathrm{H}\left(T, \mu_j - U_j^{(\mathrm{pl})}\right)\,, \tag{32}$$

$$0 = \lambda n_\mathrm{S}^\mathrm{Q}\left(T, \mu_j - U_j^{(\mathrm{pl})}\right) + (1-\lambda)n_\mathrm{S}^\mathrm{H}\left(T, \mu_j - U_j^{(\mathrm{pl})}\right)\,, \tag{33}$$

where $\lambda = V_\mathrm{Q}/V$ is the fraction of the volume occupied by the plasma phase. The phase boundaries of the coexistence region are found by putting $\lambda = 0$ for the hadron phase boundary and $\lambda = 1$ for the plasma boundary. By construction the 2P EoS results in a first-order phase transition with discontinuous behavior of energy and baryon densities.

According to the Gibbs condition [47], the number of thermodynamic degrees of freedom that may be varied without destroying the equilibrium of a mixture of r phases with n_c conserved charges is $\mathcal{N} = n_\mathrm{c} + 2 - r$. For the considered hadron–quark deconfinement transition $r = 2$. If the baryon number is the only conserved quantity, then $n_\mathrm{c} = 1$ and $\mathcal{N} = 1$. Thus, the phase boundary is one-dimensional, i.e. a line. The Maxwell construction for the first-order phase transition corresponds to $r = 2$ and $n_\mathrm{c} = 1$. When both the baryon number and strangeness are conserved, that is when $n_\mathrm{c} = 2$, one has $\mathcal{N} = 2$ and therefore the phase boundary is a surface. In such a system, a standard Maxwell construction is no longer possible [48–50][1].

When two phases coexist, the system is in general not homogeneous because the phases occupy separate domains in space. We do not, however, explicitly account for such a domain structure or a possible surface energy contribution to the equation of state. The only consequence of the phase separation in the considered 2P model is that the interaction between quasi-particles in the plasma and hadronic phase are neglected. This is different from the statistical mixed-phase model that will be discussed in the next subsection.

The resulting phase boundaries between the hadronic phase and the quark–gluon plasma in the 2P model are shown in Fig. 3. At $T = 0$ the coexistence region appears at $n_\mathrm{B}/n_0 \simeq 8$. This density is by factor two larger than the one obtained in the conventional MIT-bag-like model [26, 29]). This is because in our calculations the quarks and gluons are treated as massive quasi-particles. As it will be shown in the next section, the finite mass of the quasi-particles is needed in the quark–gluon plasma to get the EoS that is consistent with the LGT results.

2.3 The mixed-phase model

In the 2P model the interactions between quark, gluons and hadrons are entirely neglected in the coexistence region. In the following we introduce the MP model where such interactions are possible. The underlying assumption of the MP model [36–38] is that unbound quarks and gluons may coexist with hadrons forming a homogeneous quark/gluon–hadron phase. Since the mean distance between hadrons and quarks or gluons in this mixed phase may be of the same order as that between hadrons, the interaction between all these constituents (unbound quarks, gluons and hadrons) plays an important role as it defines the order of the phase transition.

[1] In [48–50] baryonic and electric charge conservation was considered in an application to the nuclear liquid–gas phase transition. As to strangeness conservation the emphasis was made mainly on the strangeness distillation effect [51]. Phase boundaries for this case were studied in detail in [52]. A more complete list of appropriate references can be found in [26].

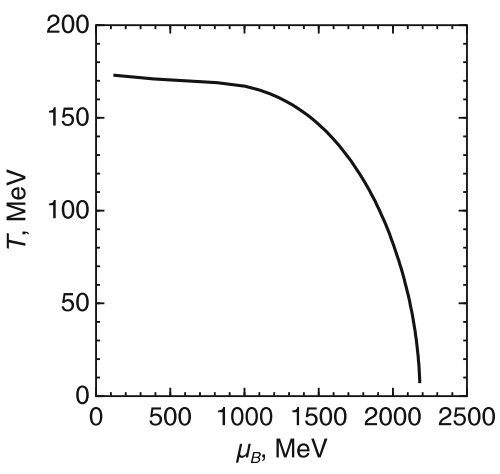

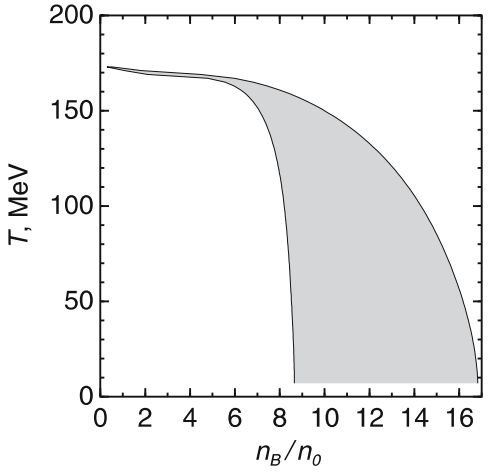

Fig. 3. The phase boundary calculated in the 2P model with the physical values of parameters as explained in Sect. 3

Under a quite general requirement for the confinement of color charges, the mean-field potential of quarks and gluons in the plasma phase is approximated by

$$U_q(\rho^{(\mathrm{pl})}) = U_g(\rho^{(\mathrm{pl})}) = \frac{\mathcal{A}}{(\rho^{(\mathrm{pl})})^\gamma} + \mathcal{B}\,(\rho^{(\mathrm{pl})})^{1/3}\,; \quad \gamma > 0\,, \tag{34}$$

where $\rho^{(\mathrm{pl})} = n_q + n_{\bar{q}} + n_g$. The second term in (34) is introduced to account for the growth of the quasi-particle mass with the density as that obtained in the HTL approximation (see (24)). The first term in (34) reflects two important limits of the QCD interactions. For $\rho^{(\mathrm{pl})} \to 0$, this potential term approaches infinity, i.e. an infinite energy is necessary to create an isolated quark or gluon that corresponds to the confinement of color objects. The other extreme limit of infinite density is consistent with the asymptotic freedom.

The generalization of the mean-field potential from (34) to the case of the mixed quark–hadron phase is obtained replacing $\rho^{(\mathrm{pl})}$ in (34) by the total density of quarks and gluons $\rho^{(\mathrm{mp})}$ with

$$\rho^{(\mathrm{mp})} = \rho_q + \rho_{\bar{q}} + \rho_g + \eta \sum_j \nu_j \rho_j \equiv \rho^{(\mathrm{pl})} + \eta\rho^{(h)}\,. \tag{35}$$

The presence of the total number density $\rho^{(\mathrm{mp})}$ in (34) implies interactions between all components of the mixed phase. For $\eta = 0$ there is no interaction between hadrons and unbound quarks and gluons. This case corresponds to such a strong binding of the hadron constituents that the presence of free color charges in their surrounding does not result in their color polarization, i.e. hadrons remain color neutral and do not see quarks and gluons outside the hadron. Thermodynamically, the potential with $\eta = 0$ implies a first-order phase transition. For $\eta = 1$ there is a very strong color polarization of hadrons. Consequently, there is no difference between bound and unbound quarks and gluons. This approximation was used in [36–38]. Here we consider η as a free parameter that is chosen in a way so as to reproduce the LGT results for the QCD equation of state.

The hadronic potential in the Hamiltonian (1) was described by a non-linear mean-field model. However, the presence of unbound quarks and gluons will modify this hadronic interaction due to the polarization of color charges. Thus, in general,

$$U_j^{(\mathrm{mp})} = U_j^{(h)} + U_j^{(h-\mathrm{pl})}\,. \tag{36}$$

The constraints imposed by the thermodynamic consistency conditions (3) can be used to find the potential for the interaction of unbound quarks/gluons with hadrons to be [36–38]

$$U_j^{(\mathrm{h\text{-}pl})} = \nu_j\eta\left(\frac{\mathcal{A}}{(\rho^{(\mathrm{mp})})^\gamma} - \frac{\mathcal{A}}{(\eta\rho^{(h)})^\gamma} + \mathcal{B}\left[(\rho^{(mp)})^{1/3} - (\eta\rho^{(h)})^{1/3}\right]\right)\,. \tag{37}$$

Consequently, the pressure and the energy density in the MP model are obtained from

$$p^{\mathrm{MP}}\left(T, \mu_j - U_j^{(\mathrm{mp})}\right) = \sum_{j\in g,q,\bar{q}} p_j\left(T, \mu_j - U_j^{(\mathrm{mp})}\right) + \sum_{j\in h} p_j\left(T, \mu_j - U_j^{(\mathrm{mp})}\right) - C(\rho^{(\mathrm{mp})})\,, \tag{38}$$

$$\varepsilon^{\mathrm{MP}}\left(T, \mu_j - U_j^{(\mathrm{mp})}\right) = \sum_{j\in g,q,\bar{q}} \varepsilon_j\left(T, \mu_j - U_j^{(\mathrm{mp})}\right) + \sum_{j\in h} \varepsilon_j\left(T, \mu_j - U_j^{(\mathrm{mp})}\right) + C(\rho^{(\mathrm{mp})})\,, \tag{39}$$

where

$$C(\rho^{(\mathrm{mp})}) = \frac{x\alpha}{\alpha+1}(\rho^{(h)})^{\alpha+1} - \rho^{(h)}F(\rho^{(h)}) + \int_0^{\rho^{(h)}} F(t)\,\mathrm{d}t - \frac{\gamma\mathcal{A}}{1-\gamma}\left[(\rho^{(\mathrm{mp})})^{1-\gamma} - (\rho^{(h)})^{1-\gamma}\right] + \frac{\mathcal{B}}{4}\left[(\rho^{(\mathrm{mp})})^{4/3} - (\eta\rho^{(h)})^{4/3}\right]\,. \tag{40}$$

The MP model described above exhibits a crossover deconfinement phase transition. The transition temperature T_c corresponds to a maximum in the T-dependence of the

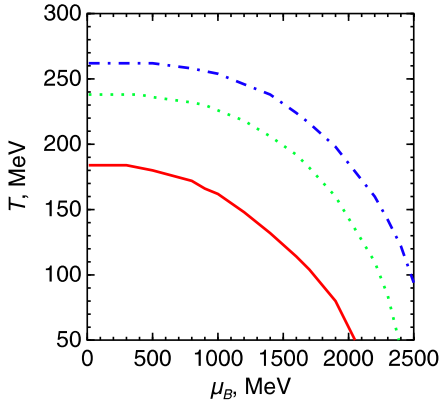

Fig. 4. The phase boundary calculated in the MP model (*solid line*). The *dotted* and *dot-dashed lines* correspond to the state where with the fraction of unbound quarks is 0.5 and 0.6, respectively

heat capacity at the given value of $\mu_{\rm B}$ (see the next section). The resulting phase boundary is shown in Fig. 4. At $T \lesssim 50$ MeV the maximum of the heat capacity is not well defined. The calculation in Fig. 4 was performed with the physical values of the parameters as introduced in the next section.

In the MP model, hadrons survive at $T > T_{\rm c}$. If the fraction of unbound quarks is defined as $\rho^{\rm (pl)}/(\rho^{\rm (pl)}+\rho^{(h)})$, then one can see from Fig. 4 that at $\mu_{\rm B}=0$ and the temperature as high as $T-T_{\rm c}\sim 100\,$MeV there are still 40% quarks that are bounded inside hadrons.

3 The comparison with the lattice data

The lattice gauge theory is the only approach that allows one to extract the physical EoS of the QCD medium. To further constrain the phenomenological models for the EoS introduced in the last section, we will compare their predictions with the available LGT results. We focus mainly on the recent LGT findings obtained in $(2+1)$-flavor QCD at the finite temperature and chemical potential [5, 6].

In order to use the mixed-phase and 2P models for the further comparison with lattice results one needs, however, to take into account that lattice calculations are generally performed with quark masses heavier than those realized in nature. Consequently, the hadron mass spectrum generated on the lattice is modified.

In [5, 6] the ratio of the pion mass m_π to the mass of the ρ meson is around 0.5–0.75, which is roughly 3 times larger than its physical value. Thus, to compare the model predictions with LGT results the hadron mass spectrum used in the model calculations should be properly scaled. For this we use the phenomenological parametrization of the quark mass dependence of the hadron masses $m_j(x)$ that was shown in [20–22] to be consistent with the MIT-bag-model results as well as with LGT findings. For the non-strange hadrons this parametrization reads [20–22]

$$\frac{m_j(x)}{\sqrt{\sigma}} \simeq \nu_{lj} a_1 x + \frac{m_j/\sqrt{\sigma}}{1+a_2x+a_3x^2+a_4x^3+a_5x^4}\,. \tag{41}$$

Here $x \equiv m_\pi/\sqrt{\sigma}$, ν_{lj} is the number of light quarks inside the non-strange hadron (i.e. $\nu_{lj}=2$ for mesons and $\nu_{lj}=3$ for baryons) and $\sigma = (0.42\,{\rm GeV})^2$. The parameters in the denominator are tabulated in Table 1.

For strange hadrons that carry strangeness $s_j=1$ and $s_j=2$ we have, respectively,

$$\frac{m_j(x)}{\sqrt{\sigma}} = 0.55\nu_{lj}x + \frac{1.7\cdot 0.42 m_j/\sqrt{\sigma}}{(1+0.068x)}\,, \quad \text{for } s_j=1\,, \tag{42}$$

$$\frac{m_j(x)}{\sqrt{\sigma}} = 0.5788x + \frac{0.42 m_j\sqrt{\sigma}}{(0.4758+0.0142x)}\,, \quad \text{for } s_j=2\,. \tag{43}$$

Simultaneously with the change of the hadron mass spectrum with the pion mass one needs to account for the shift of the transition temperature $T_{\rm c}$ with m_π. We use the parametrization that is extracted from LGT calculations [20],

$$\left(\frac{T_{\rm c}}{\sqrt{\sigma}}\right)_{m_\pi/\sqrt{\sigma}} \simeq 0.4+0.04(1)\,\left(\frac{m_\pi}{\sqrt{\sigma}}\right)\,. \tag{44}$$

To compare our phenomenological model EoS with that obtained on the lattice in [5, 6] we use the modified hadron mass spectrum form (41)–(43) corresponding to the pion $m_\pi \simeq 508\,$MeV as fixed in these LGT calculations. In the deconfined phase the current quark masses and gluon mass are in general also free parameters. In the present calculations we fixed $m_u = m_d = 65\,$MeV, $m_s = 2.08\,m_u$ and $m_g \simeq 700\,$MeV as followed from the successful description of the quark sector of the above LGT data in terms of the quasi-particle model [11].

We look for a phase transition at the appropriate temperature $T_{\rm c}$ defined by (44) by varying mainly the bag constant B in the 2P model or the strength parameter $\mathcal{A}$ in the mixed-phase model. The further fine tuning is carried out by means of the remaining parameters (one parameter in the 2P model and three for the mixed-phase model) to get the best description of LGT findings on temperature dependence of different thermodynamical quantities.

Table 1. Parameters of the interpolation formula (41)

a_1	a_2	a_3	a_4	a_5
0.51 ± 0.1	$\frac{a_1\nu_{lj}\sqrt{\sigma}}{m_j}$	0.115 ± 0.02	-0.0223 ± 0.008	0.0028 ± 0.0015

In the 2P model, where the two phases do not interact with each other, the critical temperature T_c is governed mainly by the value of the bag constant B and the parameter α that characterizes the hardness of the EoS. Choosing $B^{1/4} = 223\,\mathrm{MeV}$ and $\alpha = 2.1$ one gets $T_c \approx 176\,\mathrm{MeV}$ and $\varepsilon/T^4\,|_{T_c} = 7.84$ to be consistent with the LGT results. We have to stress, however, that for some values of the parameters, e.g. for too heavy masses, the set of equations (31)–(33) may have no solution.

In the MP model the critical temperature is defined at the position of the maximum of the heat capacity

$$c_V = \partial\varepsilon/\partial T|_{V=\mathrm{const}}\,.$$

The value of T_c depends mainly on parameters that quantify the quark/gluon interactions. With $\mathcal{A}^{1/(3\gamma+1)} = 270\,\mathrm{MeV}$ and $\gamma = 0.3$ the accepted value of the critical temperature is seen in Fig. 5 to be 188 MeV. As was noted in [26], $\gamma = 1/3$ corresponds to a string-like quark interaction.

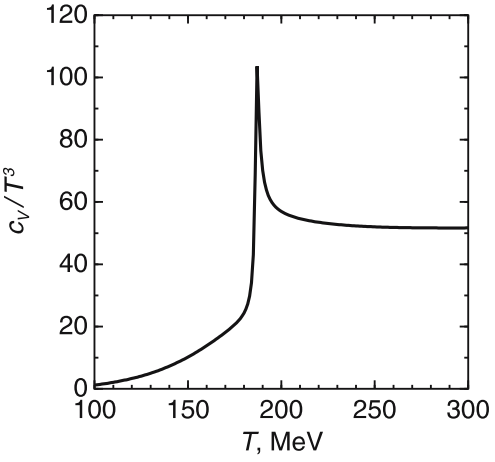

Fig. 5. Temperature dependence of the reduced heat capacity at $\mu_B = 0$

In Figs. 6 and 7 we show the comparison of the MP and the 2P model predictions with the LGT data obtained for the thermodynamic pressure p/T^4 and the energy density ε/T^4 at finite T but for $\mu_B = 0$.

The lattice calculations in [5, 6] were done on the lattices with $N_t = 4$ temporal extension. To account for the finite size effects, the LGT results have to be extrapolated to the continuum limit corresponding to $N_t \to \infty$. In general, such a procedure requires detailed LGT calculations on the lattices with different N_τ. In [5, 6], to account approximately for the finite size effect, the $N_\tau = 4$ data for the basic thermodynamic quantities were corrected being multiplied by the constant factors: $c_0 = 0.518$ and $c_\mu = 0.446$ for $\mu_B = 0$ and $\mu_B \neq 0$, respectively. These factors were determined from the ratios of the Stefan–Boltzmann ideal-gas limit for the thermodynamic pressure to its corresponding values calculated on the lattice with $N_t = 4$.

As it is seen in Fig. 6, a smooth T-dependence of the pressure in a deconfined phase may be quite well reproduced within both the MP and the 2P model. However, in the hadronic phase, that is, for $T/T_c < 1$, the models overestimate the LGT results from [5, 6]. In Fig. 6 also shown are the LGT results for $(2+1)$-flavor QCD at $\mu_B = 0$ from the Bielefeld group [53]. Improved gauge and staggered fermion actions were used there on the lattices with temporal extent of $N_t = 4$ and $N_t = 6$. These data were also extrapolated to the chiral limit [53]. As seen in Fig. 6, the Bielefeld data exhibit a smaller limiting pressure as compared to [5, 6] and essentially higher pressure in the hadronic sector, though the pion mass is $m_\pi = 770\,\mathrm{MeV}$ in the latter calculations. Our models are seen in Fig. 6 to coincide with the Bielefeld results in the confined phase. The strongly suppressed pressure at $T \leq T_c$ found in [5, 6] is non-physical and could be partly related with a too much simplified procedure to extrapolate the LGT results to a continuum limit when applying the same constant scaling factor for all values of temperatures.

The energy density shown in Fig. 7 behaves differently in the MP and 2P model. As it is expected in the 2P model, which exhibits the first-order phase transition, ε/T^4 suffers a jump at the critical temperature. This jump corresponds

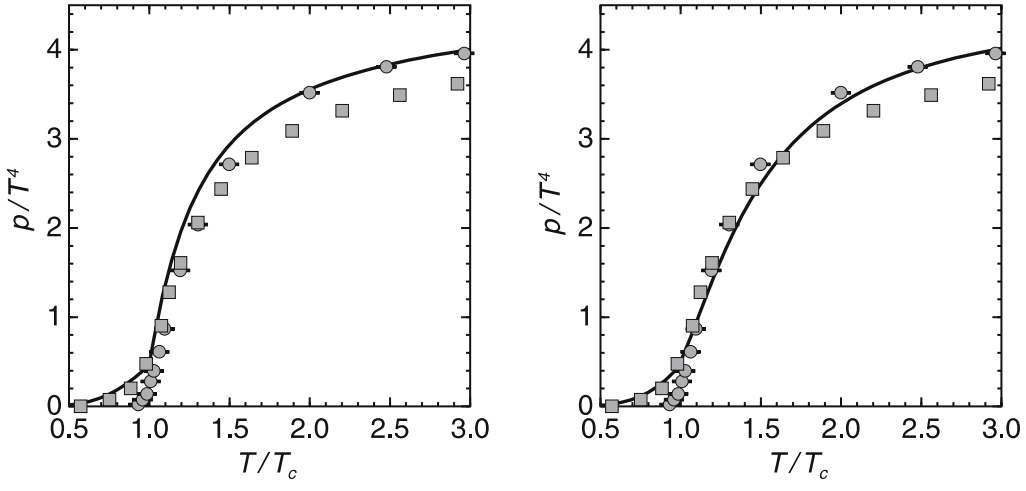

Fig. 6. The reduced pressure at $\mu_B = 0$ in 2P (the *left panel*) and MP (the *right panel*) models. *Circles* are the lattice data for the $(2+1)$-flavor QCD system [5, 6] multiplied by c_0, *squires* are the Bielefeld group data for the same case [53] (see also results cited in [20])

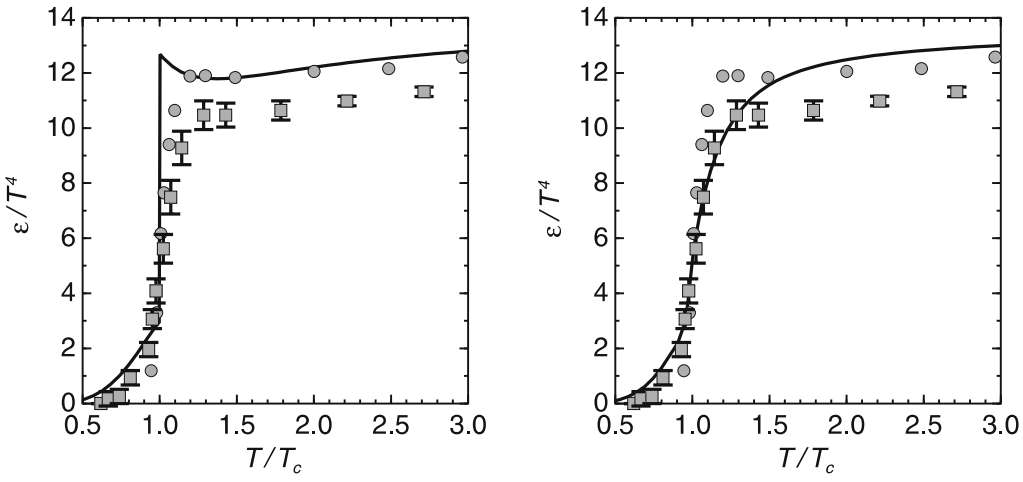

Fig. 7. The reduced energy density at $\mu_B = 0$ in the 2P (*left panel*) and MP (*right panel*) models. Notation is the same as in Fig. 6

to an energy density change by $\Delta\varepsilon \sim 0.9\,\mathrm{GeV/fm^3}$. The LGT results on the temperature dependence of ε/T^4 are seen in Fig. 7 to be noticeably better reproduced within the MP than within the 2P model. This is because the MP model exhibits a crossover-type transition as also found in the above LGT calculations. The difference between the LGT results obtained with an improved and standard action is also seen on the level of energy density.

Having established the model parameters at $\mu_B = 0$ we can further study the model comparisons with the LGT results at finite baryon density. The temperature dependence of pressure and energy density for finite values of μ_B is shown in Figs. 8 and 9 in terms of the "net baryonic pressure" $\Delta p/T^4 = (p(T,\mu_B) - p(T,\mu_B = 0))/T^4$ and the "interaction measure" $\Delta/T^4 = (\varepsilon - 3p)/T^4$.

The T-dependence of $\Delta p/T^4$ for different values of μ_B is quite well reproduced by both the MP and 2P model. The fall of $\Delta p/T^4$ for $T \geq T_c$ is entirely determined by the value of the coupling g that describes the strength of the interactions of quasi-particles and their effective mass. The observed fall does not require any artificial reduction of the number of quark–gluon degrees of freedom. It turns out that in both models a similar value of $g = 0.5$ is necessary to reproduce the LGT results.

The interaction measure Δ/T^4 exhibits a rather sharp maximum slightly above T_c with the shape of the T-dependence weakly changing with μ_B. In general, both models reproduce the above properties of the interaction measure. However, quantitatively the Δ/T^4 is overestimated in the 2P model and underestimated in the MP model near the maximum.

The interaction measure characterizes the strength of the interactions in a system. It is equal to zero for the EoS of the ultrarelativistic ideal gas of massless particles where $\varepsilon = 3p$. In the considered 2P model and at $T > T_c$ we are dealing with a gas of massive quarks and gluons interacting via a HTL-like potential (24). In contrast, in the MP model at $T > T_c$, there are interacting unbound quarks, gluons and bound quarks within the hadrons. The fraction of the bound quarks amounts in about 85% at $T \sim T_c$ (which allows one to describe this region in terms of the resonance gas model [20–22]) and almost vanishes at $3T_c$ ($\sim 5\%$). In this context the quark–gluon plasma may be considered as a strongly interacting correlated system [54–57]. In the confined phase there is an admixture of quarks at $T < T_c$ until about $0.9\,T_c$. This property of the model is very essential for a possible explanation of the "horn" structure in the K^+/π^+ excitation function [58] due to manifestation

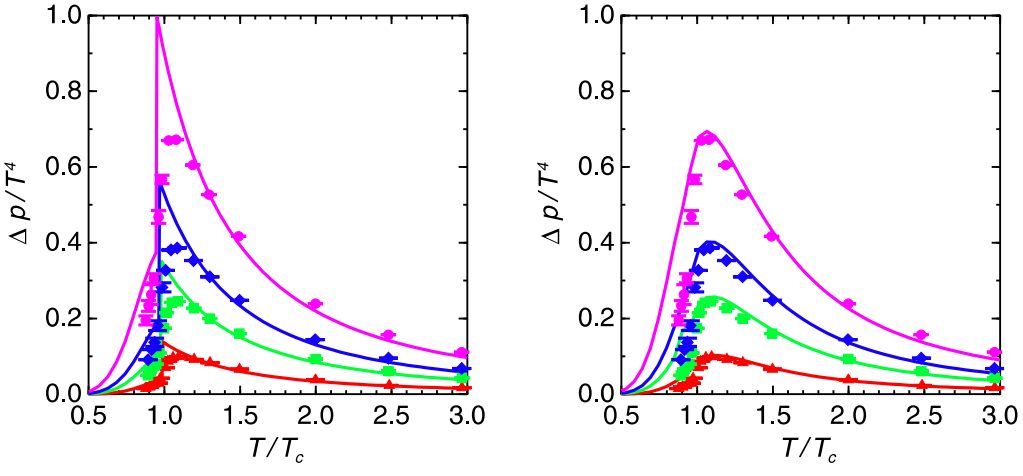

Fig. 8. Temperature dependence of the reduced pressure $(p(\mu_B) - p(0))/T^4$ at the baryon chemical potential $\mu_B =$ 210, 330, 410 and 530 MeV (from the *bottom*) within 2P (the *left panel*) and MP (the *right panel*) models. *Points* are lattice data for the $(2+1)$-flavor system [5, 6] multiplied by c_μ

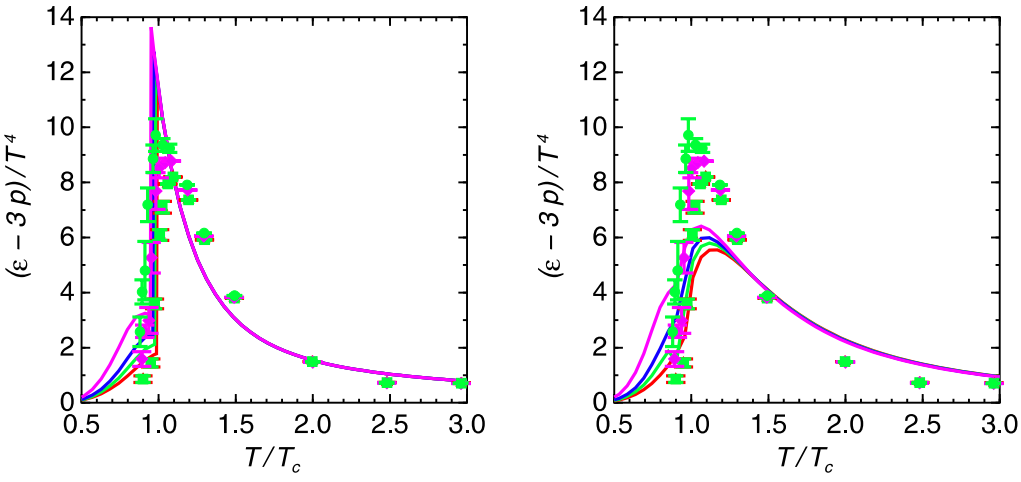

Fig. 9. Temperature dependence of the interaction measure $(\varepsilon - 3p)/T^4$ at the baryon chemical potential $\mu_B = 210$, 330, 410 and 530 MeV (from the *bottom*) within 2P (the *left panel*) and MP (the *right panel*) models. *Points* are lattice data for the $(2+1)$-flavor QCD system [5, 6] multiplied by c_μ

of the strangeness distillation effect near the critical end point [59].

The model comparison with the LGT results for the baryon density is shown in Fig. 10. It is clear from this figure that in the hadronic sector the baryon density n_B/T^3 obtained on the lattice is smaller than that predicted by the models. However, above T_c there is quite a good agreement of the model with the LGT results. This is particularly the case for the MP model which shows a better description of the LGT data near the phase transition.

In our models the absolute values of $\Delta p/T^4$, Δ/T^4 and n_B/T^3 are strongly affected by the parameter η appearing in (35). In the actual calculations $\eta = 0.025$; thus, it is essentially smaller than $\eta = 1$ as was found in our earlier parametrization based only on the LGT data obtained for $\mu_B = 0$ [26]. If $\eta = 1$ is to be substituted in our actual calculations, then all the above quantities would increase by a factor of two.

The properties and the behavior of the LGT thermodynamics at finite T and μ_B have been recently discussed in the context of the Polyakov-loop-extended Nambu and Jona–Lasinio (PNJL) model [18]. This PNJL model represents a minimal synthesis of the spontaneous chiral symmetry breaking and confinement. The model correctly describes the pion properties but obviously is not applicable near the nuclear ground state. It also does not contain the resonance contributions to the QCD thermodynamics nor the hadronic correlations below and above T_c that are essential near the phase transition. Nevertheless, the PNJL model reproduces the LGT data [3, 4] obtained in 2-flavor QCD on the pressure difference and the quark number density at various temperatures and chemical potentials remarkably well [18]. However, in the PNJL model the interaction measure Δ/T^4 was found to be underestimated by $\sim 25\%$ similarly as seen in Fig. 9 from our MP model comparison with the $(2+1)$-flavor QCD results obtained in LGT.

The phenomenological models considered here describe the EoS of the QCD matter in a broad range of thermal parameters that includes the hadronic and quark–gluon plasma phase. These models are also applicable in cold nuclear matter as they satisfy essential phenomenological constraints expected near nuclear saturation. In heavy-ion collisions, dense QCD matter created in the initial stage is expected to thermalize and expand without further generation of the entropy S. In the realistic expansion scenario some particles may be created and/or absorbed implying changes in the total entropy of the system. In general, it is

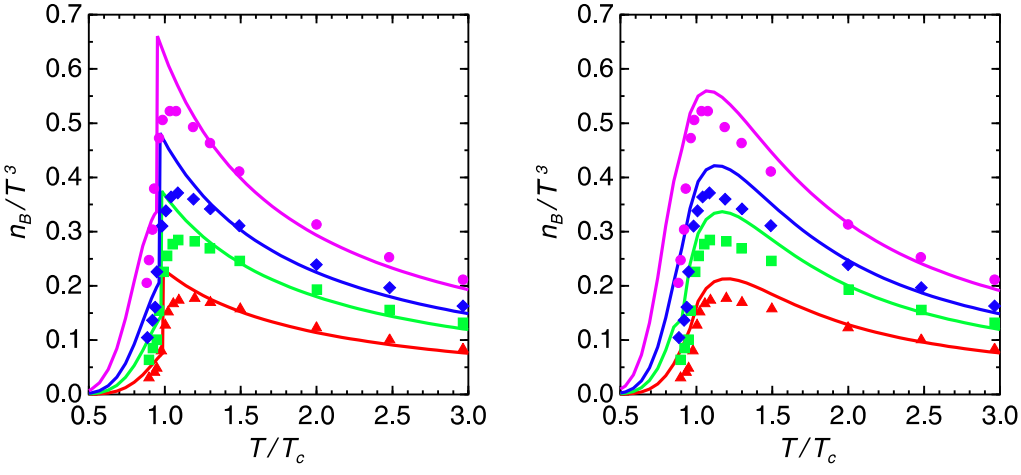

Fig. 10. Temperature dependence of the baryon density at the baryon chemical potential $\mu_B = 210$, 330, 410 and 530 MeV (from the *bottom*) in 2P (the *left panel*) and MP (the *right panel*) models. *Points* are lattice data for the $(2+1)$-flavor QCD system [5, 6] multiplied by c_μ

more convenient to consider the EoS at fixed entropy per baryon ($S/N_{\rm B}$). This thermodynamic quantity should be strictly conserved in an equilibrium case and is also less affected by any possible particle losses or creation during the expansion stage. The predictions of our models for the evolution path in the $(T, \mu_{\rm B})$-plane as obtained from the condition of fixed $S/N_{\rm B}$ is shown in Fig. 11. There are still no such isentropic lattice data for $(2+1)$-flavor system. Recently, the isentropic EoS was obtained on the lattice for 2-flavor QCD at finite $\mu_{\rm B}$ [60, 61]; however, these were still for a non-physical mass spectrum that corresponds to the pion mass $m_\pi \simeq 770$ MeV. These data are plotted in Fig. 11 together with our model results obtained with the EoS parameters that are fixed for $m_\pi \simeq 508$ MeV and for $(2+1)$-flavor system.

In general, in the high-temperature deconfined phase, one should not expect a large difference between 2- and $(2+1)$-flavor thermodynamics. The value of the quark mass in the quark–gluon plasma is also not relevant thermodynamically if $m_q/T < 1$. In the hadronic phase the number of quark flavors as well is not essential and leads only to a moderate change of the global thermodynamics. However, here the value of the quark/pion mass is of particular importance as it influences the hadronic mass spectrum. Due to the non-physical and still large pion mass used in the actual LGT calculations it is not straightforward to associate the values of the reduced entropy with the specific bombarding energy. In particular, as noted in [60, 61], the correspondence of $S/N_{\rm B} = 30$, 45 and 300 to the AGS, SPS and RHIC energies, respectively, is only a rough approximation. The QGSM transport model results [63] for central Pb+Pb collisions at top SPS energy show that the isentropic regime is reached after about 1 fm/c with $S/N_{\rm B} \approx 25$. Also calculations performed in terms of a 3-fluid relativistic hydrodynamic model show

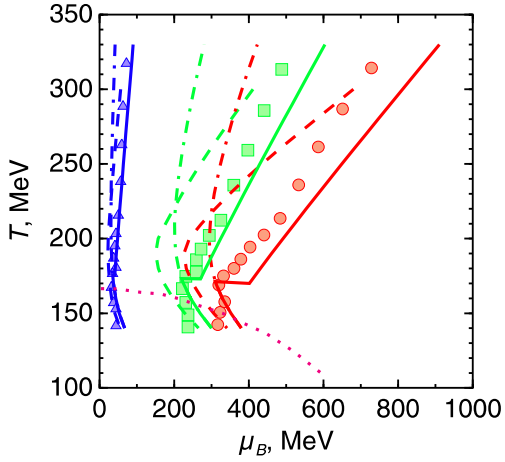

Fig. 11. Phase trajectories in the T–$\mu_{\rm B}$ representation. *Circles*, *squares* and *triangles* are the lattice 2-flavor QCD results [60, 61] for $S/N_{\rm B} = 30$, 45 and 300, respectively. The $(2+1)$-flavor model predictions are plotted by *solid* (2P EoS), dashed (MP EoS) and *dot-dashed* (Hadronic EoS) *lines* for every value of the reduced entropy. The *dotted line* parameterizes the freeze out *curve* [62]

that the isentropic expansion of central Pb+Pb collisions at the bombarding energy of 158 and 30 AGeV results in $S/N_{\rm B} \approx 30$ and 15 [64], respectively. Thus, the above dynamical models imply noticeably lower values of $S/N_{\rm B}$ than that obtained within the actual LGT calculations [60, 61]. The main origin of the above differences is related with the still too large quark mass used on the lattice.

As seen in Fig. 11 the MP and 2P models reproduce the general trend of the lattice trajectories. The lattice evolution paths are just between the 2P and MP model predictions. With increasing $S/N_{\rm B}$ these differences are noticeably smaller. The hadronic EoS predicts higher initial temperatures; however, all three phenomenological models give similar results for the freeze-out temperature. It is interesting to see in Fig. 11 that the irregularity appearing near the turning point of the lattice trajectory correlates with the flattening of the T-dependence in the Gibbs mixed phase resulting in the 2P model.

The phenomenological model results discussed so far were obtained assuming the hadronic mass spectrum that corresponds to the pion mass $m_\pi = 508$ MeV. The extrapolation of the EoS to the physical limit is quite straightforward. It amounts to replacing the $m_j(m_\pi)$ masses by their physical values. The quark and gluon masses are kept the same as being extracted from the LGT data. This approximation is justified since the change of m_q in the interval $5 < m_q < 70$ MeV does not influence the thermodynamics in the plasma phase [11] very much. Clearly, taking the physical limit in the EoS also requires one to account for the shift in $T_{\rm c}$. In the 2P model the critical temperature is recalculated according to (44) and fitted in the model by the bag constant B and the coupling g to satisfy also the condition that the critical energy density $\varepsilon_{\rm c}/T_{\rm c}^4 \simeq 6 \pm 2$ as found in LGT [20]. Within the 2P model the physical limit is achieved choosing $B^{1/4} = 207$ MeV and $g = 0.7$ which results in $T_{\rm c} = 173.3$ MeV and $\varepsilon_{\rm c}/T_{\rm c}^4 = 7.83$.

The extrapolation of the MP model EoS to the physical limit is less transparent due to a rather strong non-linear relation between the hadronic and plasma phase. In this model the physical limit is approximately accounted for by replacing the LGT mass spectrum by its physical form. All further parameters that are required in the MP model to quantify the EoS are kept the same as that found in the comparison of the model predictions with the LGT results. With the above chosen model parameters the crossover deconfinement transition appears at $T_{\rm c} = 183$ MeV. Note that the phase boundaries in the preceding section were calculated for these physical parameters of the EoS.

4 Summary

We have formulated two different phenomenological models for the equation of state within the quasi-particle approximation of the QCD matter: the two phase (2P) model with the first-order deconfinement transition and the mixed-phase (MP) model in which the transition from hadronic phase to quark–gluon plasma is of the crossover type.

In our approach both the hadronic and the quark–gluon plasma phase are considered to be non-ideal systems. The interactions between the constituents are included within the mean-field approximation. The modified mean-field Zimanyi model is applied to describe the interacting resonance gas component. In this approach, the saturation properties of the symmetric nuclear matter in the ground state are reproduced correctly and the Danielewicz constraints resulting from heavy-ion collision data at intermediate energies are well fulfilled.

The quark–gluon phase in the 2P model is constructed as a massive quasi-particle system supplemented by the density-dependent potential term which simulates the HTL interactions. The first-order phase transition from the hadronic phase to the deconfined quark–gluon plasma is constructed within the 2P model by means of the Gibbs phase equilibrium conditions.

In the MP model the coexistence and correlations between quarks/qluons and hadrons are assumed near deconfinement. In addition to the HTL-like interaction term a string-like interaction is introduced between both unbound quarks/qluons and quarks that are confined within hadrons. In this model we are dealing with strongly interacting QCD matter which exhibits a crossover-type deconfinement phase transition.

The models are constructed in a way thermodynamically consistent and reproducing the properties of the EoS as calculated on the lattice. The limited set of model parameters is defined from the constraints imposed by the recent lattice data on the temperature and chemical potential dependence of the basic thermodynamical observables. The comparison of the model predictions with the LGT data was performed within the same set of approximations as used on the lattice. Of particular importance is the correct treatment of the hadronic mass spectrum which in the LGT calculations is non-physical due to the still too large value of the quark mass.

Keeping in mind the principal difference between the first-order and crossover-type phase transition, both the 2P and MP model were shown to provide a quite satisfactory description of the LGT thermodynamics for $(2+1)$-flavor QCD. Both models reproduce the T- and μ_{B}-dependence of the main thermodynamic quantities in a broad range of thermal parameters. The observed deviations of the model predictions from the lattice results near T_{c} and in the hadronic sector for the $(2+1)$-flavor case may be, to a large extent, attributed to uncertainties in the LGT data due to the finite size effect. The predicted isentropic trajectories in the phase diagram were shown to be consistent with that recently calculated on the lattice within the 2-flavor QCD.

The phenomenological equations of state constructed here satisfy all physically relevant constraints expected in the cold and excited nuclear matter. These EoS can be applied in a broad parameter range that covers the region of the deconfinement transition in QCD. Thus, both the MP and 2P EoS could be used as input in dynamical models that describe the space-time dynamics and the evolution of the medium created in heavy-ion collisions. Within hydrodynamic models our EoS can be important to study the role and the influence of deconfinement and the order of the phase transition on the physical observables. Such studies are in progress.

Acknowledgements. We are grateful to D.B. Blaschke, Y.B. Ivanov, V.N. Russkikh, S.A. Sorin and D.N. Voskresensky for interesting discussions and comments. This work was supported in part by the Deutsche Forschungsgemeinschaft (DFG project 436 RUS 113/558/0-3), the Russian Foundation for Basic Research (RFBR grants 06-02-04001 and 05-02-17695) by the special program of the Ministry of Education and Science of the Russian Federation (grant RNP.2.1.1.5409) and by the Polish Committee for Scientific Research (KBN-2P03B 03018).

References

1. F. Wilczek, hep-ph/0003183
2. F. Karsch, AIP Conf. Proc. **602**, 323 (2001)
3. C.R. Allton, S. Ejiri, S.J. Hands, O. Kaczmarek, F. Karsch, E. Laermann, C. Schmidt, Phys. Rev. D **68**, 014 507 (2003)
4. C.R. Allton, S. Ejiri, S.J. Hands, O. Kaczmarek, F. Karsch, E. Laermann, K. Redlich, Phys. Rev. D **71**, 054 508 (2005)
5. Z. Fodor, Nucl. Phys. A **715**, 319 (2003)
6. F. Csikor, G.I. Egri, Z. Fodor, S.D. Katz, K.K. Szabo, A.I. Toth, JHEP **405**, 46 (2004)
7. P. Lévai, U. Heinz, Phys. Rev. C **57**, 1879 (1998)
8. A. Peshier, B. Kämpfer, O.P. Pavlenko, G. Soff, Phys. Rev. D **54**, 2399 (1996); A. Peshier, B. Kämpfer, G. Soff, Phys. Rev. C **61**, 045 203 (2000)
9. A. Peshier, B. Kämpfer, G. Soff, Phys. Rev. D **66**, 094 003 (2002)
10. M. Bluhm, B. Kämpfer, G. Soff, Phys. Lett. **620**, 131 (2005)
11. K.K. Szabó, A.I. Tóth, JHEP **306**, 008 (2003)
12. A. Rebhan, P. Romatschke, Phys. Rev. D **68**, 025 022 (2003)
13. J. Cleymans, K. Redlich, H. Satz, E. Suhonen, Z. Phys. C **33**, 151 (1986)
14. D.B. Blaschke, K.A. Bugaev, Fizika B **13**, 491 (2004)
15. D.B. Blaschke, K.A. Bugaev, Prog. Part. Nucl. Phys. **53**, 197 (2004)
16. R.A. Schneider, W. Weise, Phys. Rev. C **64**, 055 201 (2001)
17. T. Renk, R.A. Schneider, W. Weise, Phys. Rev. C **66**, 014 902 (2002)
18. M.A. Thaler, R. Schneider, W. Weise, Phys. Rev. C **69**, 035 210 (2004)
19. Y. B Ivanov, V.V. Skokov, V.D. Toneev, Phys. Rev. D **71**, 014 005 (2005)
20. F. Karsch, K. Redlich, A. Tawfik, Eur. Phys. J. C **29**, 549 (2003)
21. F. Karsch, K. Redlich, A. Tawfik, Phys. Lett. B **571**, 67 (2003)
22. S. Ejiri, F. Karsch, K. Redlich, Phys. Lett. B **633**, 275 (2006)
23. C. Ratti, M.A. Thaler, W. Weise, Phys. Rev. D **73**, 014 019 (2006)
24. N.G. Antoniou, F.K. Diakonos, A.S. Kapoyannis, Nucl. Phys. A **759**, 417 (2005)
25. M. Bluhm, B. Kämpfer, G. Soff, hep-ph/0402252
26. V.D. Toneev, E.G. Nikonov, B. Friman, W. Nörenberg, K. Redlich, Eur. Phys. J. C **32**, 399 (2003)

27. P. Danielewicz, R. Lacey, W.G. Lynch, Science **298**, 1592 (2002)
28. P. Danielewicz, nucl-th/0512009
29. Y.B. Ivanov A.S. Khvorostukhin, E.E. Kolometsev et al., Phys. Rev. C **72**, 025 804 (2005)
30. T. Klähn, D. Blaschke, S. Typel et al., nucl-th/0602038
31. J.P. Blaizot, E. Iancu, A. Rebhan, Phys. Rev. D **63**, 065 003 (2001)
32. A. Peshier, B. Kämpfer, G. Soff, Phys. Rev. C **61**, 045 203 (2000)
33. A. Peshier, B. Kämpfer, G. Soff, Phys. Rev. D **66**, 094 003 (2002)
34. J. Letessier, J. Rafelski, Phys. Rev. C **67**, 031 902 (2003)
35. A. Chodes, R.L. Jaffe, K. Johnson, C.B. Thorn, Phys. Rev. D **10**, 2599 (1974)
36. E.G. Nikonov, A.A. Shanenko, V.D. Toneev, Heavy Ion Phys. **8**, 89 (1998)
37. E.G. Nikonov, V.D. Toneev, A.A. Shanenko, Yad. Fiz. **62**, 1301 (1999) [translated as Physics of Atomic Nuclei, **62**, 1226 (1999)]
38. V.D. Toneev, E.G. Nikonov, A.A. Shanenko, in: Nuclear Matter in Different Phases and Transitions, ed. by J.-P. Blaizot, X. Campi, M. Ploszajczak (Kluwer Academic Publishers, Dordrecht Boston London, 1999), p. 309
39. A.A. Shanenko, E.P. Yukalova, V.I. Yukalov, Yad. Fiz. **56**, 151 (1993)
40. A.A. Shanenko, E.P. Yukalova, V.I. Yukalov, Nuovo Cim. A **106**, 1269 (1993)
41. A.A. Shanenko, E.P. Yukalova, V.I. Yukalov, Physica A **197**, 629 (1993)
42. J. Zimányi, B. Lucács, P. Lévai et al., Nucl. Phys. A **484**, 647 (1988)
43. R. Rapp, J. Wambach, Phys. Rev. C **53**, 3059 (1996)
44. J.O. Andersen, E. Braaten, E. Petitgirard, M. Strickland, Phys. Rev. D **66**, 085 016 (2002)
45. J.O. Andersen, E. Braaten, M. Strickland, Phys. Rev. Lett. **83**, 2139 (1999)
46. J.O. Andersen, E. Braaten, M. Strickland, Phys. Rev. D **62**, 045 004 (2000)
47. L.D. Landau, E.M. Lifshitz, Statistical Physics, Vol. 5, Part 1 (Pergamon Press, Oxford, 1980)
48. N. Glendenning, Phys. Rev. D **46**, 1274 (1992)
49. N. Glendenning, Phys. Rep. **342**, 393 (2001)
50. C. Ducoin, P. Chomaz, F. Gulminelli, Nucl. Phys. A **771**, 68 (2006)
51. C. Greiner, P. Koch, H. Stöcker, Phys. Rev. Lett. **58**, 1825 (1993)
52. K.S. Lee, U. Henz, Phys. Rev. D **47**, 2068 (1993)
53. F. Karsch, E. Laermann, A. Peikert, Nucl. Phys. B **605**, 579 (2001)
54. E.V. Shuryak, I. Zahed, Phys. Rev. C **70**, 021 901 (2004)
55. E.V. Shuryak, I. Zahed, J. Phys. G: Nucl. Partic. **34**, S1221 (2004)
56. G.E. Brown, C.-H. Lee, M. Rho, hep-ph/0402207
57. D.N. Voskresensky, Nucl. Phys. A **744**, 378 (2004)
58. NA49 Collaboration, M. Gazdzicki et al., J. Phys. G **30**, S701 (2004)
59. V.D. Toneev, A.S. Parvan, J. Phys. G: Nucl. Partic. **31**, 583 (2005)
60. S. Ejiri, F. Karsch, E. Laermann, C. Schmidt, Phys. Rev. D **73**, 054 506 (2006)
61. F. Karsch, hep-lat/0601013
62. J. Cleymans, K. Redlich, Phys. Rev. Lett. **81**, 5284 (1998)
63. V.V. Skokov, V.D. Toneev, Phys. Rev. C **73**, 021 902 (2006)
64. Y.B. Ivanov, V.N. Russkikh, V.D. Toneev, Phys. Rev. C **73**, 044 904 (2006)